The Meteoritical Society

Meteoritics & Planetary Science 43, Nr 1/2, 285–298 (2008)
Abstract available online at http://meteoritics.org

TOF-SIMS analysis of cometary particles extracted from Stardust aerogel

Thomas STEPHAN[1†*], George J. FLYNN[2], Scott A. SANDFORD[3], and Michael E. ZOLENSKY[4]

[1]Institut für Planetologie, Westfälische Wilhelms-Universität Münster, Wilhelm-Klemm-Str. 10, 48149 Münster, Germany
[2]Department of Physics, SUNY Plattsburgh, Plattsburgh, New York 12901, USA
[3]Astrophysics Branch, NASA Ames Research Center, Moffett Field, California 94035, USA
[4]Astromaterials Research and Exploration Science, NASA Johnson Space Center, Houston, Texas 77058, USA
[†]Present address: Department of the Geophysical Sciences, University of Chicago, 5734 South Ellis Avenue, Chicago, Illinois 60637, USA
[*]Corresponding author. E-mail: tstephan@uchicago.edu

(Submitted 12 December 2006; revision accepted 22 June 2007)

Abstract–Sections of seven cometary fragments extracted from the aerogel collector flown on the Stardust mission to comet 81P/Wild 2 were investigated with TOF-SIMS. These grains showed a rather heterogeneous chemical and mineralogical composition on a submicrometer scale. However, their average chemical composition is close to bulk CI chondritic values, which is consistent with analyses of numerous Stardust samples using various techniques. As a result, the TOF-SIMS analyses support the conclusion that Wild 2 has a CI-like bulk composition. The cometary particles resemble anhydrous chondritic porous interplanetary dust particles, which have previously been suggested to originate from comets. For one of the fragments, polycyclic aromatic hydrocarbons that could possibly be attributed to the comet were observed.

INTRODUCTION

Cometary dust particles were collected during flyby at comet 81P/Wild 2 in January 2004 and safely returned to Earth in January 2006 by NASA's space mission Stardust (Brownlee et al. 2003, 2006; Tsou et al. 2003). The primary capture medium for the cometary dust was low-density silica aerogel with a total exposed surface area of 1039 cm^2.

In order to determine their elemental, isotopic, mineralogical, and organic properties, individual fragments of cometary particles were extracted from the aerogel. Subsequently, these grains were embedded in epoxy and sliced with an ultra-microtome to provide samples from each cometary fragment for a multitude of analytical techniques.

In the present study, time-of-flight secondary ion mass spectrometry (TOF-SIMS) was used to analyze particle sections provided either as microtome sections or potted butts that remained after sectioning away about one half of the respective particle.

SAMPLES

The eight samples investigated in this study are from seven cometary fragments that were extracted from three different tracks in Stardust aerogel (Table 1). All three tracks showed fragmentation of the original impacting cometary particle, and the samples investigated in this study are fragments from various localities along the tracks.

Two samples are from Track 2 in a loose chip of aerogel (FC3) that was found on the surface of the avionics deck in the interior of the sample canister upon opening. This piece of aerogel has not been tied to a specific aerogel cell, but almost certainly came from the cometary tray, whose exposed face was stowed against the avionics deck when the Sample Return Capsule (SRC) was closed after cometary encounter. Three terminal grains from this ~400 μm long, carrot-shaped track were removed, embedded in epoxy, and microtomed. From the first grain, the potted butt (FC3,0,2,1,0) was investigated after preparation of several microtome slices. From the second grain, a TEM grid with several microtome slices (FC3,0,2,2,3) was studied.

Two samples are from Track 44 from aerogel cell C2004. This track is the largest impact feature in the entire cometary tray (Fig. 1). The impacting cometary particle struck the edge of the tray frame and then bounced into the adjacent aerogel. Here the tray frame is covered by aluminum foil (Al 1100; >99% pure). The main purpose of the foils was to facilitate the removal of the aerogel tiles from the modular collector trays following return to Earth (Tsou et al. 2003), but they served also as a capture medium (Hörz et al. 2006; Leitner et al. 2008). Five grains were pulled from the track without removing the cell from the tray. Both samples analyzed in this study are from grain #4. One is a potted butt (C2004,1,44,4,0), and the second is a TEM grid (C2004,1,44,4,5) with microtome slices from the other half of the grain.

Finally, from Track 35 extracted from aerogel cell C2054,

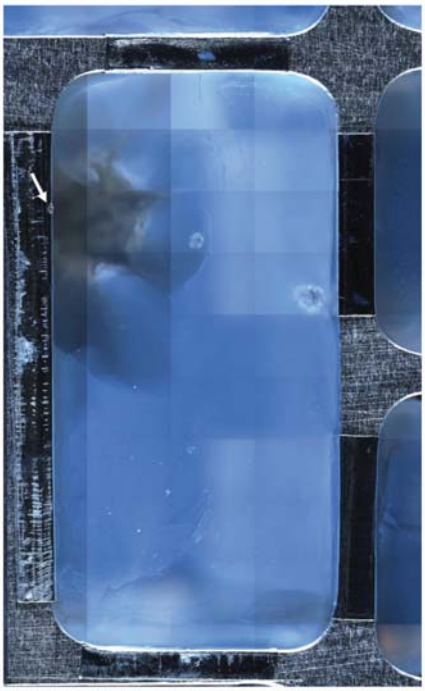

Fig. 1. Optical image of aerogel cell C2004 from NASA-Johnson Space Center (JSC) level 2 photo documentation using reflected light. The cell is 4 cm high and 2 cm wide. Track 44 is the large impact feature in the upper left. The impacting particle struck the edge of the tray frame (white arrow) before bouncing into the aerogel.

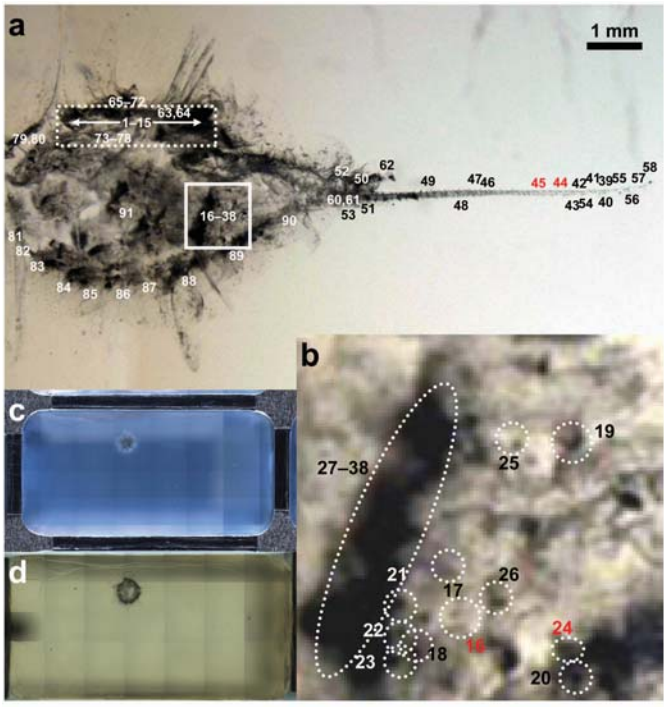

Fig. 2. a) Track 35 from aerogel cell C2054. Positions of fragments extracted from this track are shown. A region in the bulbous part of the track (solid square) from which grains 16–38 were extracted is enlarged in (b). Grains #16 and #24 from that region as well as grains #44 and #45 from the stylus were investigated in this study. Figures 2c and 2d show the aerogel cell C2054 during NASA-JSC level 2 (reflected light) and level 3 (backlight) photo documentation, respectively.

four different fragments were investigated, two as microtome sections on TEM grids from grains #16 (C2054,0,35,16,9) and #24 (C2054,0,35,24,5), and two as potted butts from grains #44 (C2054,0,35,44,0) and #45 (C2054,0,35,45,0). The track, ~1.17 cm long, and the position of the various fragments before extraction are shown in Fig. 2. Grains #16 and #24 were extracted from the wall of the bulbous part of the track, whereas grains #44 and #45 are from the stylus that leads toward the terminal grain.

EXPERIMENTAL TECHNIQUES

A TOF-SIMS IV instrument from ION-TOF was used in this study. Prior to measurement, all analyzed surfaces were cleaned by Ar^+ ion sputtering, although sputtering is known to destroy organic molecules by fragmentation. However, cleaning was required because all sample surfaces showed an omnipresent, mainly organic contamination layer preventing any SIMS analysis of the particle sections. For the analyses, an intermittent Ga^+ primary ion beam with a pulse length of 1.5 ns and a beam diameter of ~300 nm was used. With a repetition rate of 10 kHz, the analyzed sample regions were raster-scanned either with 128^2 pixels, 128 shots per pixel in each scan, and a total of 200 scans, or 256^2 pixels, 64 shots per pixel in each scan, and a total of 100 scans. Each stack of images was corrected for apparent sample shift resulting from instrument instabilities over the approximately 12-hour-long measurements before being added together. Both polarities, positive as well as negative secondary ions, were analyzed in two consecutive measurements. Further details on the TOF-SIMS technique are given by Stephan (2001).

For quantification of the results, relative sensitivity factors obtained from glass standards that are usually used for quantitative TOF-SIMS analysis of silicates (Stephan 2001) were applied. Usually, Si is used as reference element in TOF-SIMS of minerals, but this could not be done in this case because the aerogel capture medium is compositionally identical to SiO_2 and all investigated samples contain residual aerogel intermingled with the particles. Therefore, all quantitative results in this study are given as atomic element ratios relative to Mg. The uncertainty for such an approach is expected to be on the order of a factor of <1.5. Even for non-silicate particles, the derived metal-to-magnesium ratios should be of comparable accuracy.

Fe could have been the choice of reference element rather than Mg for TOF-SIMS elemental abundance quantification, since neither element is a significant contaminant in the aerogel. However, during data evaluation it became clear that one sample was relatively enriched in Fe, making it unsuitable as the general standard, whereas the main elemental ratios relative to Mg were all approximately chondritic.

Table 1. Samples analyzed in this study.

Sample name[a]	Sample type	Microtome slice	Size (μm)
FC3,0,2,1,0	Potted butt	–	8
FC3,0,2,2,3	Microtome sections	#14, #15, #16	9 × 5
C2004,1,44,4,0	Potted butt	–	24 × 12
C2004,1,44,4,5	Microtome sections	#47	23 × 11
C2054,0,35,16,9	Microtome sections	#44	25 × 15
C2054,0,35,24,5	Microtome sections	#20	16 × 8
C2054,0,35,44,0	Potted butt	–	20 × 15
C2054,0,35,45,0	Potted butt	–	9

[a]The prefix C2 denotes the Cometary Tray 2 (Trays 1 and 3 were flight spares) followed by a three-digit number indicating one of the 132 parent aerogel cells in the collector. In the case of loose chips that cannot be assigned to a specific cell, the sample name starts with the name of the chip, e.g., FC3. The second part of the sample name is the number of aerogel piece separated from the aerogel cell or chip. "0" stands for the parent cell or chip. The third part of the sample name is the sequential track number. Sub-samples taken from the track are numbered, the fourth part of the sample name. Further subdividing of specific grains is mentioned in the last part of the sample name. Here "0" stands for potted butts. For example "C2004,1,44,4,5" is the TEM grid 5, prepared from grain 4, extracted from Track 44, which was located in aerogel piece 1 removed from aerogel cell C2004.

The amount of aerogel in each sample can be assessed by assuming a chondritic Si/Mg ratio (0.931; Anders and Grevesse 1989) for the sample, and attributing the excess Si to aerogel. Although Stardust aerogel is known to be contaminated with traces of elements other than Si and O (Tsou et al. 2003), no blank correction was applied, in contrast with the one used in a companion study, where cometary matter was analyzed directly in aerogel tracks (Stephan et al. 2008). There, element ratios in the aerogel blank were found to vary by up to a factor of five, even for samples from the same aerogel cell, and up to a factor of 60, when samples from different cells are compared. In the present study, no blank aerogel material from the respective particle tracks was available that would have allowed to perform a reliable blank correction.

RESULTS AND DISCUSSION

TOF-SIMS secondary ion images for all cometary fragments analyzed are provided in Figs. 3–10. In addition, Fig. 11 displays TOF-SIMS three-color composite images for all samples, where red, green, and blue are assigned to the normalized intensities of Mg, Ca, and Fe, respectively. Also shown in Fig. 11 are outlines of the Si distributions. For most particles, the Si distribution significantly extends beyond the locations of the other major rock-forming elements, illustrating that most particles are probably covered by compacted aerogel from the capture process.

For the calculation of quantitative data, regions of interest were selected from Figs. 3–10 using the distributions of major elements like Mg, Al, Ca, and Fe. The Si distribution was not considered in these cases. The outlines of the regions of interest are also shown in Fig. 11.

Quantitative results are plotted in Fig. 12 as element ratios relative to Mg and normalized to CI chondritic ratios, and are also listed in Table 2 as element ratios without CI normalization (CI reference data are given for comparison). CI chondritic abundances are used as an approximation for solar system abundances (Anders and Grevesse 1989). This neither implies that Wild 2 dust is expected to be mineralogically similar to CI chondrites, nor does this introduce a preconception regarding Wild 2 element ratios.

Since no reliable blank correction was possible, it has to be noted that the quantitative analysis of some elements may be compromised based on the contamination observed in other Stardust aerogel samples (Stephan et al. 2008). Taking these observations into account, up to 100% of the measured Li and Sc, up to 84% of the V, and up to 63% of the K in the present study can be attributed to the aerogel. The expected blank corrections for Na and Ti would be <20% and <14%, respectively. For other elements shown in Fig. 12, the contribution from aerogel contamination is negligible (<2%). To visualize the possible effects of aerogel blank correction, a range of expected element ratios after blank correction is shown in Fig. 12. For this correction, the span of trace element abundances observed in three aerogel samples (Stephan et al. 2008) was taken into account.

Element data for Cu, Rb, Sr, and Ba are only provided in Table 2, because these trace element data lie clearly above CI and are probably due to contamination. From the analysis of aerogel samples, no reliable data on the level of contamination for these elements in Stardust aerogel can be derived. However, from their lateral distribution these elements often seem to be correlated with alkalis, supporting the idea that they are caused by contamination.

High Si data in Table 2 clearly demonstrate that all samples investigated in this study are heavily intermingled with aerogel.

In the following, TOF-SIMS results for each sample are discussed individually.

FC3,0,2,1,0

One half of the first cometary fragment was provided as potted butt embedded in epoxy. The secondary ion distribution images (Fig. 3) show that this particle is rather heterogeneous. Ti shows a large enrichment in one region; Al and Ca together with some Na and Mg are concentrated in another. An Fe

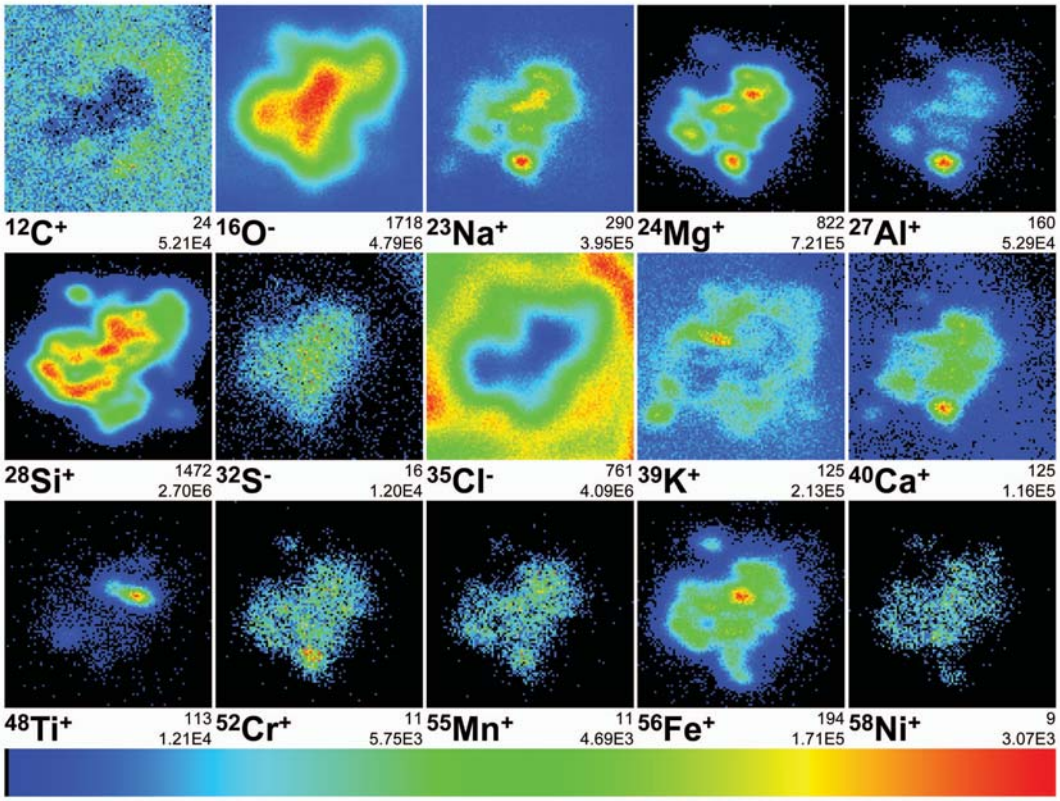

Fig. 3. Secondary ion images of the potted butt FC3,0,2,1,0. The field of view is 9 × 9 μm^2 (99 × 99 pixels, 25,600 primary ion shots/pixel). All individual ion images use the same linear color scale shown, where black corresponds to zero counts and red is used for the maximum intensity given below every image (e.g., 822 counts for $^{24}Mg^+$). The other number underneath each image is the integrated intensity of the entire field of view (e.g., 7.21 × 10^5 counts for $^{24}Mg^+$). The same labeling is used in subsequent figures containing secondary ion images.

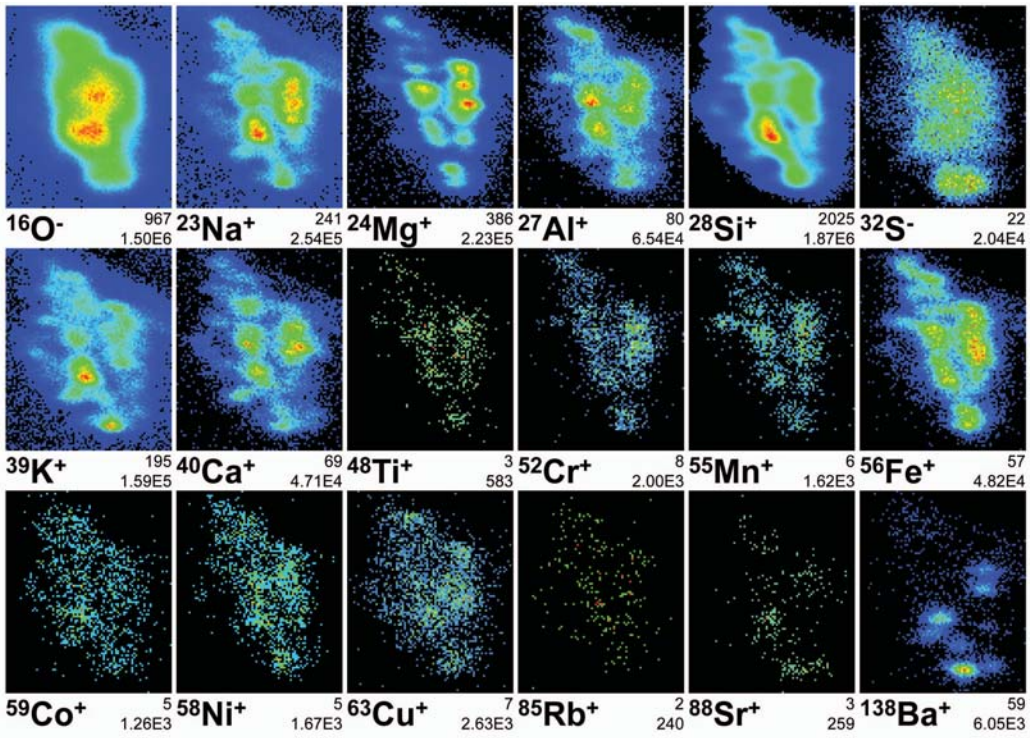

Fig. 4. Secondary ion images of thin section #15 from FC3,0,2,2,3. The field of view is 7.5 × 9 μm^2 (82 × 99 pixels, 25,600 shots/pixel).

Table 2. Atomic element ratios relative to Mg = 100.[a]

Element	CI[b]	FC3,0,2,1,0	FC3,0,2,2,3[c]	C2004,1,44,4,0	C2004,1,44,4,5	C2054,0,35,16,9	C2054,0,35,24,5	C2054,0,35,44,0	C2054,0,35,45,0
Li	0.00532	0.0104(9)	0.0093(9)	0.004(1)	0.011(1)	0.008(2)	0.017(3)	0.007(1)	0.012(4)
Na	5.34	10.36(2)	24(4)	7.23(3)	17.25(4)	25.31(9)	32.5(1)	5.04(3)	10.35(8)
Mg	100	100.0(1)	100.0(3)	100.0(3)	100.0(2)	100.0(3)	100.0(3)	100.0(3)	100.0(5)
Al	7.91	5.46(4)	28(10)	12.3(1)	28.8(1)	19.9(2)	25.7(2)	87.4(2)	7.1(2)
Si	93.1	2006(2)	7000(4000)	4810(10)	4046(3)	4253(6)	5277(6)	4877(9)	6360(10)
K	0.351	2.107(7)	7(4)	1.040(9)	1.85(1)	5.58(3)	2.42(2)	1.59(1)	1.22(2)
Ca	5.69	6.14(3)	7(1)	4.95(4)	14.51(5)	5.08(5)	7.09(6)	3.57(3)	3.90(7)
Sc	0.00318	0.0061(9)			0.012(2)			0.010(2)	0.020(8)
Ti	0.223	2.30(3)	0.35(7)	0.20(2)	1.01(5)	0.28(3)	0.31(3)	0.17(2)	0.21(3)
V	0.0273	0.012(1)	0.05(2)	0.021(4)	0.030(4)	0.039(7)	0.031(7)	0.021(4)	0.017(7)
Cr	1.26	1.08(1)	1.4(2)	1.43(3)	1.37(3)	1.26(4)	13.3(1)	1.18(3)	1.81(8)
Mn	0.889	0.90(3)	0.97(5)	0.98(3)	0.86(3)	0.85(4)	1.21(5)	1.14(5)	1.3(1)
Fe	83.8	63.0(2)	70(20)	95.7(6)	61.5(3)	49.8(4)	55.0(5)	88.7(5)	241(2)
Co	0.209	0.14(1)	1.4(6)	1.22(5)	3.15(7)	0.31(4)	0.23(3)	0.15(2)	0.18(4)
Ni	4.59	2.9(1)	5(2)	8.6(6)	5.6(4)	7.5(4)	5.8(4)	4.3(2)	9(1)
Cu	0.0486	0.055(9)	10(5)	0.16(3)	5.5(1)	7.5(3)	70(1)	2.6(1)	
Rb	0.000660		0.009(3)	0.0038(6)	0.0082(7)	0.0031(8)	0.006(1)	0.002(1)	0.009(2)
Sr	0.00219	0.0076(8)	0.05(2)	0.009(2)	0.020(2)	0.020(4)	0.022(4)	0.020(3)	0.02(2)
Ba	0.000418	0.0032(6)	1.6(6)	0.003(1)	0.116(5)	0.083(8)	0.033(5)	0.007(2)	

[a]All errors are 1σ, given as last significant digit in parentheses.

[b]According to Anders and Grevesse (1989).

[c]From sample FC3,0,2,2,3 three different microtome sections were analyzed. The values given here are geometric mean values with errors comprising the entire range of observed ratios.

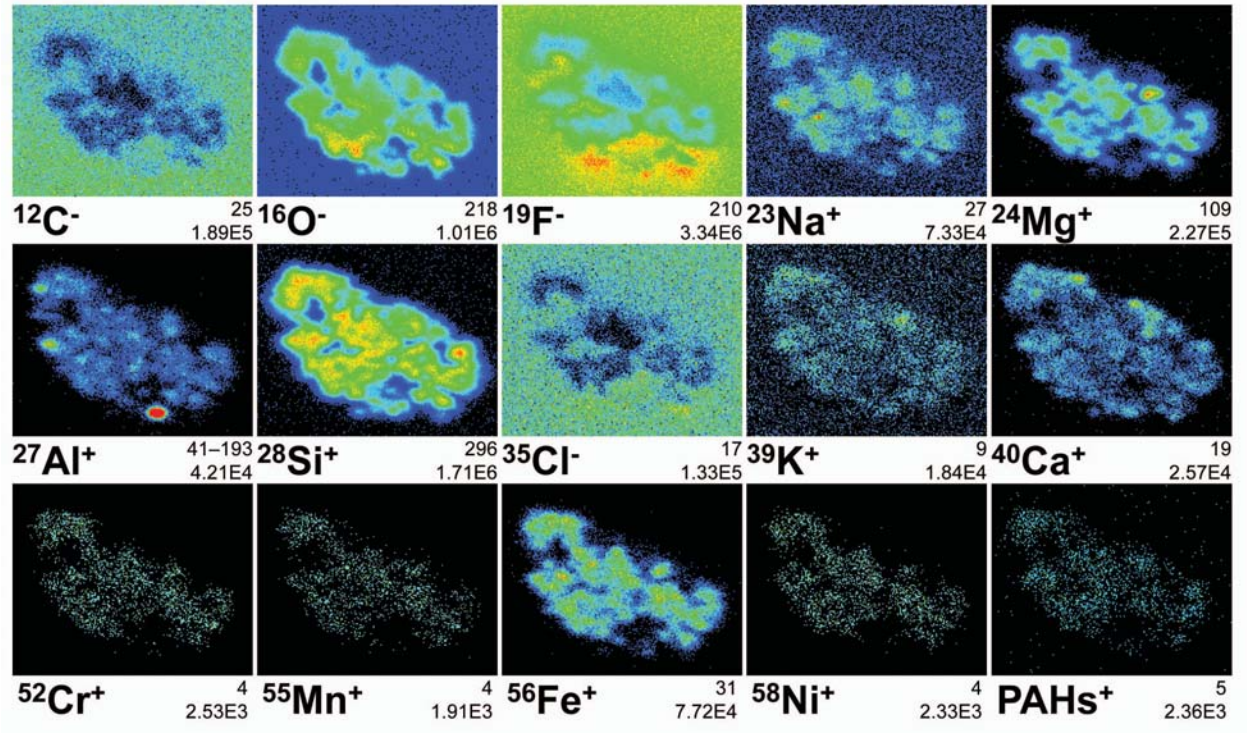

Fig. 5. Secondary ion images of potted butt C2004,1,44,4,0. The field of view is 25 × 20 μm^2 (193 × 154 pixels, 6400 shots/pixel).

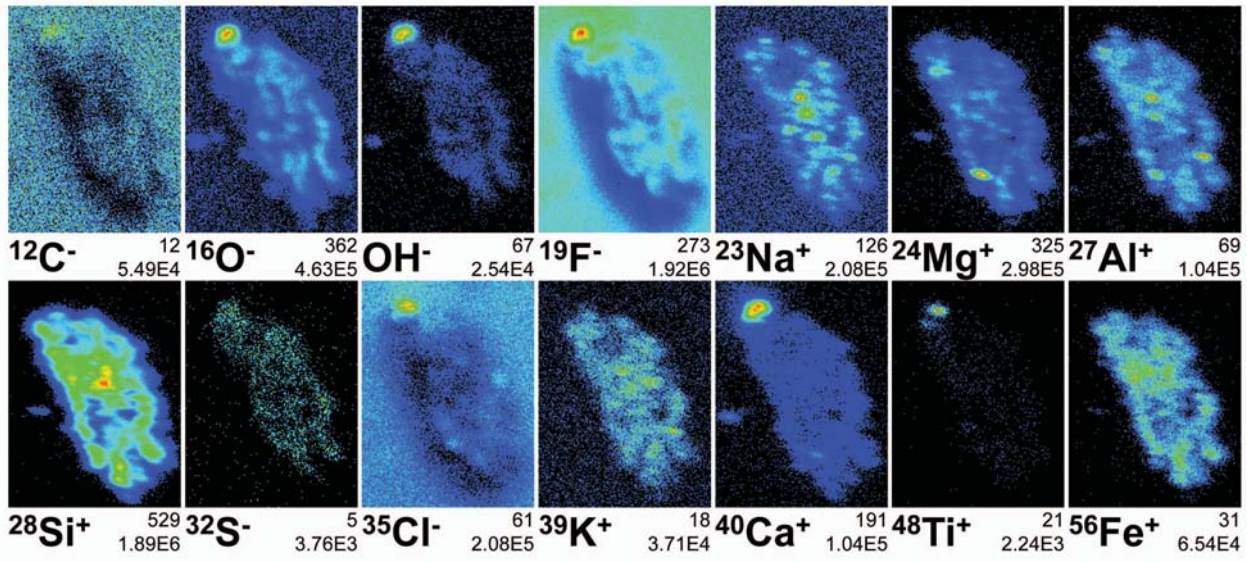

Fig. 6. Secondary ion images of thin section #47 from C2004,1,44,4,5. The field of view is 19 × 25 μm^2 (156 × 205 pixels, 6400 shots/pixel).

hotspot also shows high Mg and some correlated Ti. Cl is mainly confined to the epoxy, whereas C and K form an outer rim. This outer rim is indicative of a surface correlated enrichment of C and K that is present in the aerogel. This finding is supported by the comparison of major rock-forming elements and the outline in the Si distribution (Fig. 11).

Silicon from the aerogel dominates the composition of the sample. The Si/Mg ratio is ~20 (Table 2). However, other elements in FC3,0,2,1,0 show a CI-like pattern (Fig. 12). Li, Na, Al, Ca, Sc, Cr, Mn, Fe, Co, and Ni relative to Mg are all within a factor of two of CI. The particle shows significant enrichments in K, Ti, Sr, and Ba, and a slight depletion in V compared to CI. As mentioned above, K may be attributed to aerogel contamination, and high Ti represents an unidentified Ti-rich phase, visible in Fig. 3.

Because the lateral distribution of Si shows high concentrations not only at the margins of the particle but also in the interior, it can be deduced that this sample consists of fine-

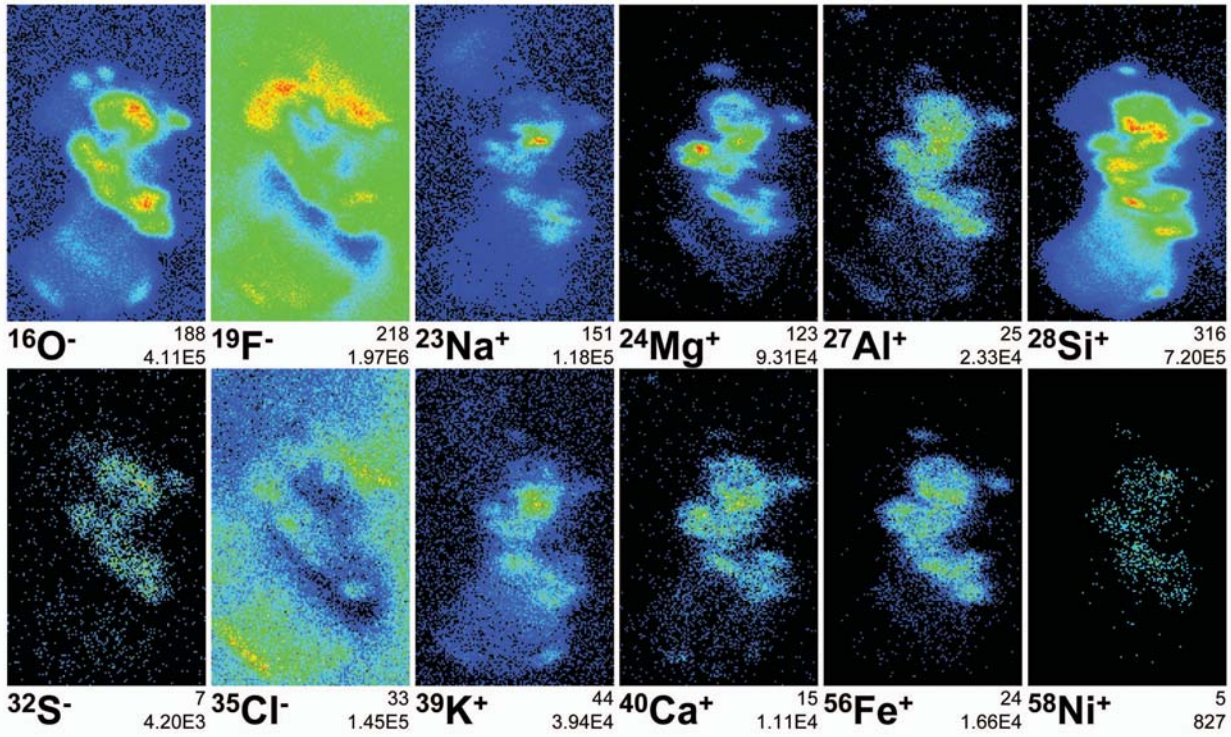

Fig. 7. Secondary ion images of thin section #44 from C2054,0,35,16,9. The field of view is 20 × 32 μm² (114 × 182 pixels, 6400 shots/pixel).

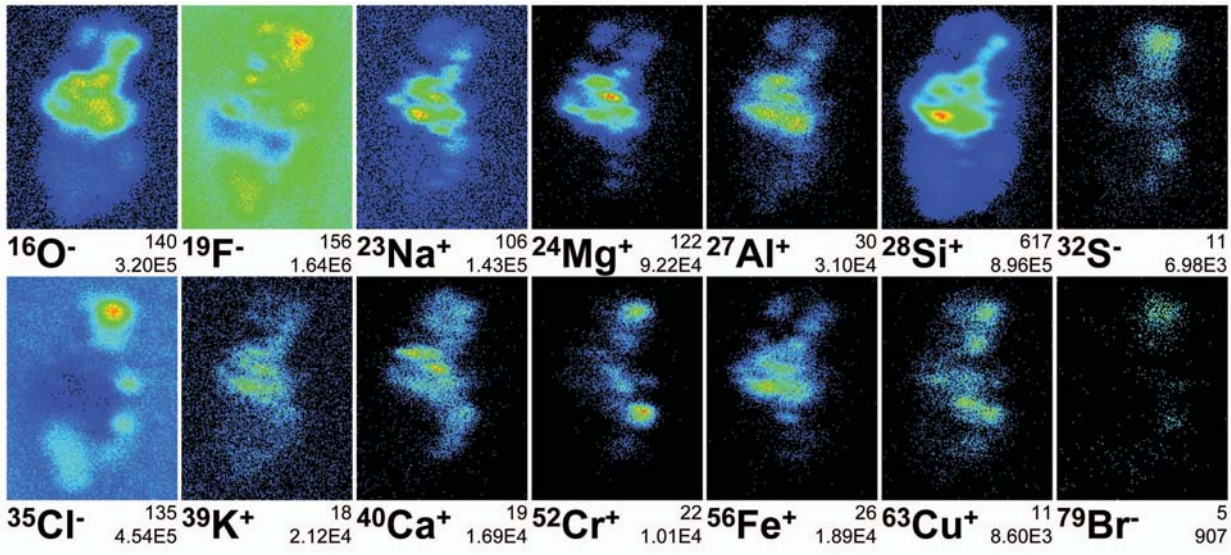

Fig. 8. Secondary ion images of thin section #20 from C2054,0,35,24,5. The field of view is 13 × 17 μm² (142 × 186 pixels, 6400 shots/pixel).

grained minerals intermingled with aerogel similar to what has been observed in other studies (Zolensky et al. 2006). Despite all structural changes during deceleration of the particle in the aerogel, the overall chondritic properties survived.

The Ca,Al-rich region, about 1 μm in diameter, may be attributed to some Ca,Al-rich mineral, such as observed in another Wild 2 sample (Zolensky et al. 2006). Although in the present case a clear mineralogical identification of this phase cannot be made from TOF-SIMS analysis alone, a similarity to Ca,Al-rich inclusions (CAIs) observed in primitive meteorites seems likely.

FC3,0,2,2,3

From the second cometary fragment from Track 2, several microtome sections on a TEM Cu-grid were available.

Three of these sections (#14, #15, and #16) were investigated by TOF-SIMS. These samples showed basically identical results. As an example, Fig. 4 shows the secondary ion distribution images from section #15. The quantitative data presented in Fig. 12 and Table 2 were obtained by calculating the geometric means of these three measurements. Errors in Table 2 include the maximum deviations for the data from the three sections compared to the geometric mean values. The data show that Li, Ca, Ti, V, Cr, Mn, Fe, and Ni relative to Mg are within a factor of two of CI chondrites. Strongly enriched (more than a factor of three) with respect to CI are Na, Al, K, Co, Cu, Rb, Sr, and Ba. Some lateral correlation to Si seems to exist for these elements, and the enrichment might therefore be attributed to aerogel contamination, especially since this sample is even more heavily dominated by Si than the other grain from the same track. It has a Si/Mg ratio of ~70.

C2004,1,44,4,0

Two different slices of the fragment #4 from Track 44 were investigated. The first sample is a potted butt embedded in epoxy. To within a factor of two, this section showed CI-chondritic abundances relative to Mg for Li, Na, Al, Ca, Ti, V, Cr, Mn, Fe, and Ni (Fig. 12). Slightly enriched (less than a factor of three) is K, while Co, Cu, Rb, Sr, and Ba are strongly enriched.

One Al hotspot was found on the surface of the grain (Fig. 5). Since this hotspot is not correlated with any other element enrichment, it is likely pure Al and may be attributed to surface contamination. Indeed, the impacting particle hit the Al foil on the frame of the Stardust Tray Assembly (STA) before entering the aerogel (Fig. 1). It is possible that the particle has acquired some Al contamination from the foil. Consequently, the region of the Al hotspot was omitted for the determination of the chemical composition in Fig. 12 and Table 2.

Based on the CI-like composition and the heterogeneous element distribution, this grain probably consists of a mixture of different minerals, including olivine, pyroxene, and feldspar, although a proper mineral identification from TOF-SIMS results alone is not possible. However, aerogel intimately mixed with the cometary matter dominates the particle as can be inferred from the Si/Mg ratio of ~48. As seen in the three-color image for this fragment (Fig. 11), the Si-rich area surrounding the particle is also enriched in Ca, an indication for some local Ca-bearing contamination of the aerogel.

C2004,1,44,4,0 was the only sample in this study that clearly showed polycyclic aromatic hydrocarbons (PAHs) to be present in the grain. The lateral distribution of PAHs is also shown in Fig. 5. For this distribution image, secondary ions from typical PAH species at masses 115 amu to 302 amu were added (Fig. 13). However, since all samples had to be sputter-cleaned by Ar bombardment prior to the actual analysis, the presence of PAHs after sputtering indicates their relatively high abundance in this sample. Unfortunately, a reliable estimate for any contribution by contamination of the aerogel to the observed PAH content cannot be made, since blank correction was not possible. The relative abundances of various PAHs in the TOF-SIMS spectrum of this sample (Fig. 13) resembles the pattern observed for material from the Allende CV3 meteorite shot into aerogel as discussed by Sandford et al. (2006).

C2004,1,44,4,5

The other sample, slice #47, from the same cometary fragment, had different characteristics. It has chondritic abundances of Li, V, Cr, Mn, Fe, and Ni relative to Mg. Overall, Ca is slightly enriched (less than a factor of three), whereas Na, Al, K, Sc, Ti, Co, Cu, Rb, Sr, and Ba show significant enrichments. Ca, Ti, and the halogens F and Cl are concentrated in one O-rich spot on the surface of this grain (Fig. 6). At first glance, from these imaging TOF-SIMS results, OH^- seems to be also enriched in the Ca spot. High OH^-/O^- ratios of the order of one are often indicative for the presence of hydrated minerals (Stephan et al. 1993). However, since the OH^-/O^- ratio is significantly below one (~0.17), the presence of a hydrous phase seems unlikely. F and Cl enrichments and their location at the very surface of the grain suggest that once again contamination is responsible for this spot, but a cometary origin cannot be unambiguously excluded. From the somewhat enriched C^- signal (Fig. 6), a Ca carbonate, cometary or terrestrial, seems to be a possible explanation. Investigation by high-resolution transmission electron microscopy reveals that this is a crystalline grain, and further analyses will allow the specific identification of the mineral phase (van der Bogert et al. 2007).

Other elements are also distributed heterogeneously. In particular, Mg has a high concentration in one distinct spot (Fig. 6). High Al, often correlated with Na and K, is also observed for some minor spots. The particle's major element composition can be explained by a mixture of olivine or pyroxene and feldspar. The Si/Mg ratio is ~40 in this sample, indicating again an intimate mixture with aerogel.

C2054,0,35,16,9

This sample is from one of two grains from the bulbous part of Track 35. Element mapping of microtome section #44 (Fig. 7) revealed some Mg-rich regions. The Mg/Fe ratio of ~2, which is the highest among all samples analyzed in this study (Table 2), may be indicative of Mg-rich olivine or pyroxene. Li, Ca, Ti, V, Cr, Mn, Fe, Co, and Ni relative to Mg are within a factor of two of CI. High Na, Al, and K in a few spots may indicate the presence of feldspar. Also strongly enriched are Cu, Rb, Sr, and Ba. Aerogel is again responsible for the high Si/Mg ratio (~43) in this sample.

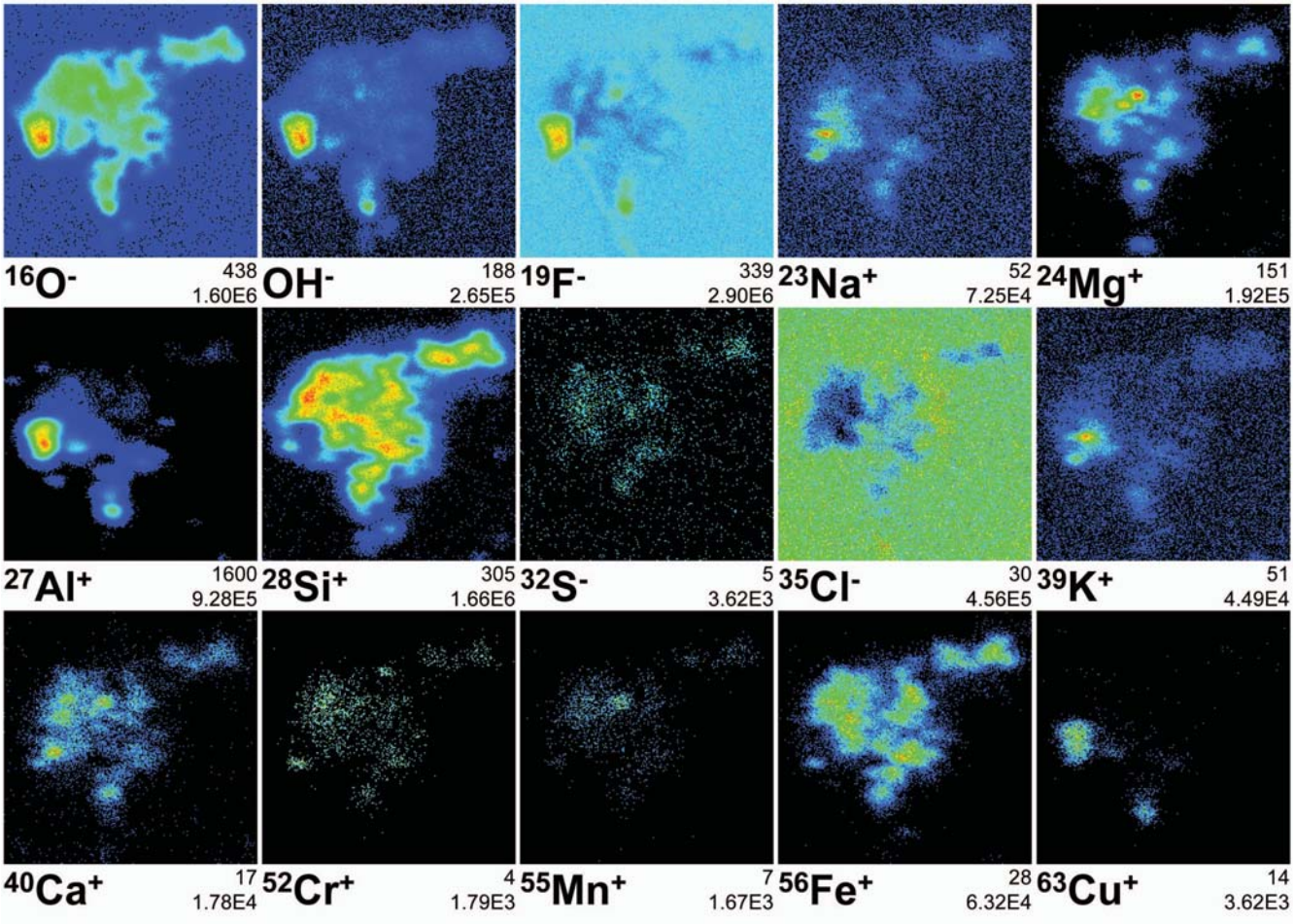

Fig. 9. Secondary ion images of potted butt C2054,0,35,44,0. The field of view is 21 × 21 μm^2 (197 × 197 pixels, 6400 shots/pixel).

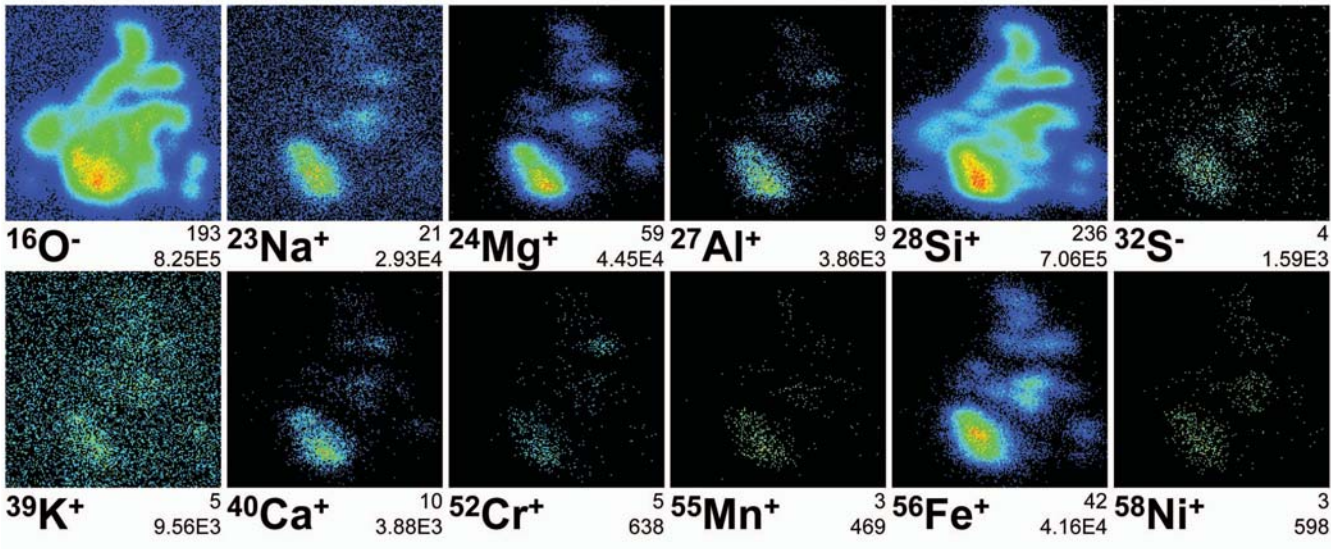

Fig. 10. Secondary ion images of potted butt C2054,0,35,45,0. The field of view is 10 × 10 μm^2 (164 × 164 pixels, 6400 shots/pixel).

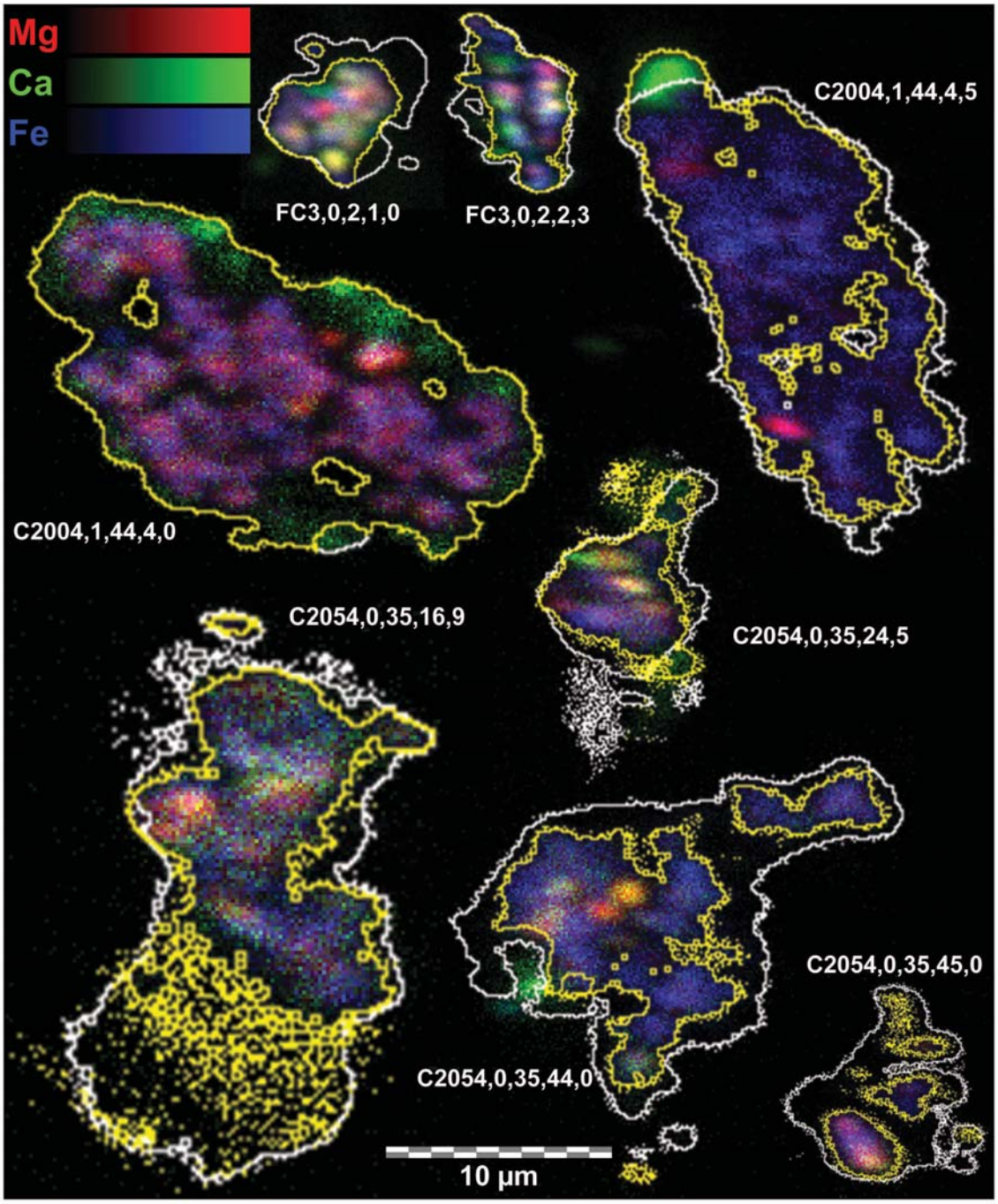

Fig. 11. TOF-SIMS three-color composite images, where red, green, and blue are assigned to the normalized intensities of Mg, Ca, and Fe, respectively. Yellow lines mark the regions of interest used to determine element ratios given in Fig. 12 and Table 2. The white lines illustrate the outlines of the Si distributions. For most particles, this distribution significantly extends the distribution of other major rock-forming elements, illustrating that most particles are probably covered by compressed aerogel from the capture process.

C2054,0,35,24,5

The other fragment from the bulbous part of Track 35 shows a very similar chemical composition. Ca, Ti, V, Mn, Fe, Co, and Ni relative to Mg are within a factor of two chondritic. The Mg/Fe ratio is ~1.8 (Table 2). Mg is enriched in one spot (Fig. 8). High Na, Al, and K abundances are observed like in the other grain from Track 35. Also enriched are Li, Rb, Sr, and Ba. Cr and Cu are strongly enriched in some regions of the particle. One of these spots is also characterized by high halogen intensities. Since these elements are often observed in different types of contaminants, it seems

Table 3. Correlation coefficients (CC) between element ratios from Table 2 (geometric mean values) and those from chondrite types (Lodders and Fegley 1998).

Chondrite type	CC	Chondrite type	CC
CI	0.994	H	0.992
CM	0.993	L	0.988
CV	0.993	LL	0.980
CO	0.993	R	0.993
CK	0.990	Acapulcoites	0.989
CR	0.992	K	0.992
CH	0.934	EH	0.962
		EL	0.993

to be unlikely that they represent cometary matter. Again a high Si/Mg ratio of ~53 was observed in this sample, indicative of aerogel.

C2054,0,35,44,0

Two cometary fragments of Track 35 were extracted from the small path that leads towards the terminal particle of that impact. Fragment #44 was provided as potted butt. As with the grains from the bulbous part of the track, C2054,0,35,44,0 shows Mg enriched in some minor spots. However, the Mg/Fe ratio is ~1.1 and therefore significantly below the ratio for the two previous particles. The elements Li, Na, Ca, Ti, V, Cr, Mn, Fe, Co, and Ni are present in abundances relative to Mg within a factor of two to CI. Slightly enriched (less than a factor of three) is Rb. Strongly enriched are Al, K, Sc, Cu, Sr, and Ba.

Al is extremely enriched in two spots that also show high Cu concentrations in addition to local enrichments of O, OH, and F (Fig. 9). Leitner et al. (2008) observed that the Stardust Al foil contains Cu impurities. Therefore, it seems plausible that the Al concentrations observed in this sample are due to contamination related to the Stardust Al foil. These regions were omitted for the calculation of element ratios. The Si/Mg ratio is ~49 in this sample, an indication of aerogel dominating the sample.

C2054,0,35,45,0

This fragment, also from the stylus of Track 35, is even more dominated by Fe. The Mg/Fe ratio (~0.4) is the lowest observed for all samples in this study. Na, Al, Ca, Ti, V, Cr, Mn, Co, and Ni relative to Mg are within a factor of two chondritic. Li and Fe are slightly enriched (less than a factor of three). Strongly enriched are K, Sc, Rb, and Sr. The Si/Mg ratio is ~64, indicative of the presence of aerogel.

From the composition of the four fragments investigated from Track 35, it can be inferred that the projectile was rather heterogeneous. While Mg-rich grains were found in the bulbous part of the track, both fragments close to the terminus have relatively high Fe contents.

Aerogel

All the samples analyzed in this study show rather high Si abundances due to aerogel in close association with the cometary fragments. These grains are not only enclosed by aerogel as can be seen in Fig. 11, but also intermingled with aerogel leading to extremely high Si/Mg ratios between 20 and 70 (Table 2). Such a close relation between cometary matter and aerogel was also observed in a companion study on fine-grained material studied directly in the aerogel tracks using TOF-SIMS (Stephan et al. 2008) as well as during the investigation of the mineralogy and petrology of the samples (Zolensky et al. 2006).

Bulk Composition

Although the composition of individual cometary fragments differs significantly from CI chondritic abundances, geometric mean values for most element ratios shown in Fig. 12 are close to solar system abundances as represented by CI values. Geometric means were chosen, because they are more robust against statistical outliers than arithmetic means. Especially for ratios, arithmetic mean values are meaningless, since they would overestimate elements that show an anti-correlation to the normalization element. Finally, arithmetic means of ratios in general differ from ratios of arithmetic means. These shortcomings are all eliminated when using geometric means.

From these geometric mean values, only K/Mg shows a large enrichment, by a factor of 6.5, compared to CI. However, K was often found to be related to contamination mainly from the aerogel. Slight enrichments (more than a factor of two, but less than a factor of three) are observed for Na, Al, and Co relative to Mg (Fig. 12). Based on the contamination observed in other Stardust aerogel samples (Stephan et al. 2008), apparent Na enrichments as well as some high Li and Ti abundances can also be assigned to aerogel contamination. Al in some cases might be connected to the Stardust Al foils. The apparent Sc enrichment can be fully explained by the fact that Sc was only detectable in particles with high Sc concentrations due to an interference with the $SiOH^+$ peak in the mass spectrum. A huge $SiOH^+$ signal resulting from the aerogel often inhibits the unambiguous detection of a small Sc^+ peak at mass 45 amu. Non-detections were not accounted for while calculating the geometric mean values. In addition, the Sc content in aerogel is only poorly known as reflected by the long vertical lines in Fig. 12. Therefore, the high Sc values can also be explained by aerogel contamination.

Cu, Rb, Sr, and Ba are only trace elements in CI chondrites, but were found in some of the samples in rather high abundances (Table 2). For some of these element enrichments, aerogel contamination or contamination of the grains during sample preparation seems to be the most

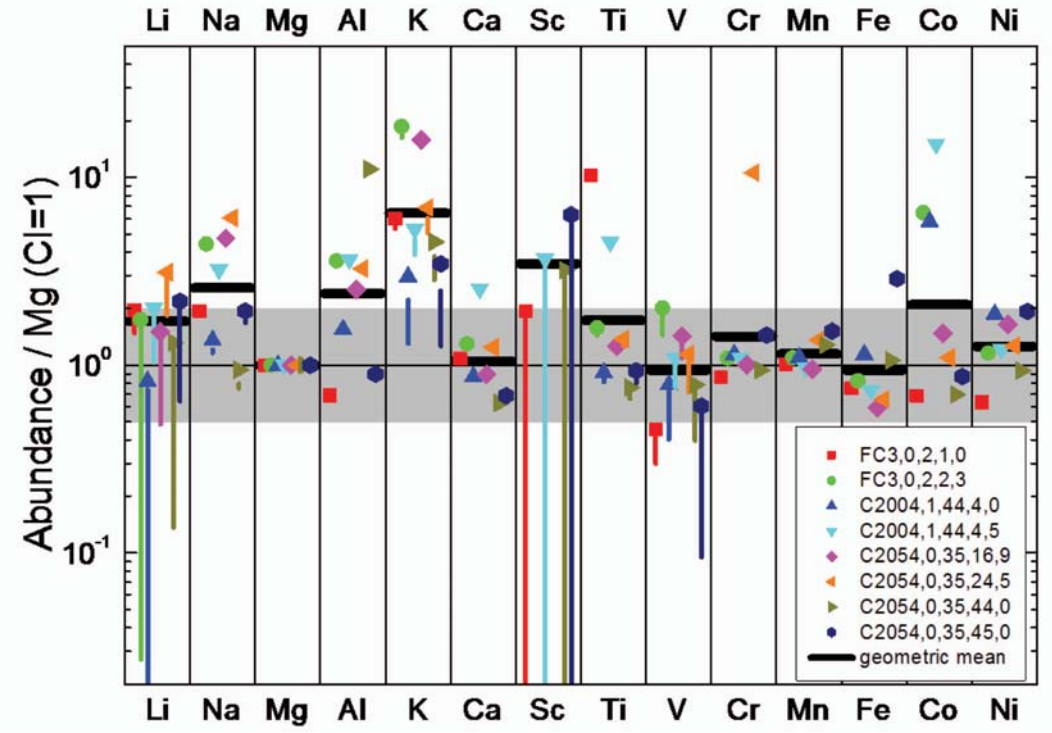

Fig. 12. Element abundances of the eight cometary fragments extracted from the Stardust aerogel capture medium relative to Mg and normalized to CI chondritic values. Vertical lines show range of expected values after correction for aerogel blank.

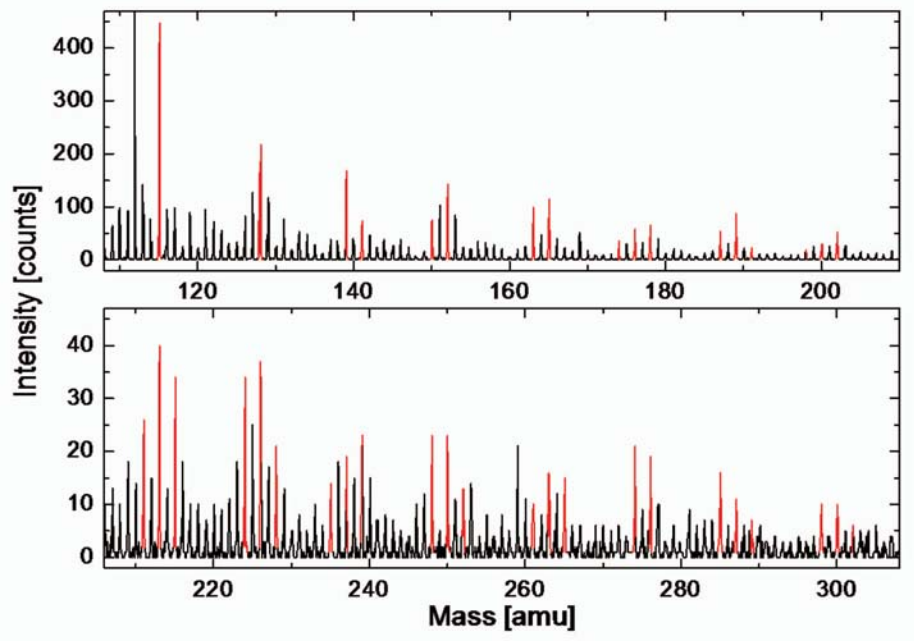

Fig. 13. TOF-SIMS mass spectrum from sample C2004,1,44,4,0 showing typical PAH mass peaks marked in red. The sum of these peaks were used to produce the distribution image in Fig. 5.

plausible explanation. However, we cannot exclude the possibility that these excesses have a cometary origin.

To evaluate the chemical resemblance with CI chondrites, element ratios from Table 2, excluding data for Si, Cu, Rb, Sr, and Ba that are probably compromised by contamination, were compared with element ratios of different chondrite classes (Lodders and Fegley 1998). Correlation coefficients were calculated between TOF-SIMS data and all chondrite classes (Table 3). Among all chondrites, the highest correlation coefficient of 0.994 was

found for CI chondrites. However, also for CM, CV, CO, CR, H, R, K, and EL chondrites, correlation coefficients of 0.992–0.993 were calculated. None of the chondrite classes yield a correlation coefficient below 0.93. These results show that from the available data set in this study, an unequivocal assignment to a specific chondrite class could not be made. For better classification, data for light elements, especially C, would be crucial. However, the data confirm the chondritic nature of Wild 2 matter and is consistent with CI or solar system abundances.

CONCLUSIONS

The TOF-SIMS investigation of eight samples from seven cometary fragments from three different tracks in Stardust aerogel clearly confirmed the heterogeneity of cometary matter collected by the Stardust mission. None of the grains showed a clear monomineralic composition. Instead, they all consist of various sub-grains that are often less than 1 μm in size and that are intimately mixed with aerogel. However, the degree of heterogeneity within the different samples seems to vary. This is also obvious from the three-color composite images in Fig. 11. The multicolored images illustrate the heterogeneous compositions of the respective grains, while the relatively monochromatic images denote a less variable mineralogy.

Although most particles showed large deviations from CI chondritic composition at least for some elements, the average composition reflected by the geometric mean values shown in Fig. 12 is close to bulk CI chondritic values that seem to represent the bulk composition of comet 81P/Wild 2 (Flynn et al. 2006). Taking into account the small number of actually analyzed particles in this study, this might be a surprising result, but it confirms the observations made in two companion studies on TOF-SIMS analysis of cometary residues on Stardust Al foil (Leitner et al. 2008) and on ultra fine-grained cometary matter in Stardust aerogel tracks (Stephan et al. 2008), both revealing the CI chondritic nature of Wild 2 on a micrometer scale.

The study of organic compounds in the samples was hampered by the presence of organic contamination probably from sample preparation as well as from hydrocarbons inherent in the aerogel. However, for one of the fragments, polycyclic aromatic hydrocarbons that could possibly be attributed to the comet were observed.

From the fine-grained nature of all investigated samples, their CI chondritic bulk composition, the lack of high OH^-/O^- ratios that would be indicative for hydrated mineral phases, and the presence of organic matter, the cometary fragments seem to most closely resemble chondritic porous interplanetary dust particles (CP-IDPs), fine-grained aggregates of anhydrous minerals like olivine and pyroxene, Fe sulfides, glass, and carbonaceous material, which have previously been suggested to originate from comets (Brownlee et al. 1994; Bradley 1994). Individual CP-IDPs that are typically 10 μm in size show a similar variability in their bulk composition (Schramm et al. 1989) as observed in the present study for cometary fragments with comparable sizes.

Acknowledgments–We thank Keiko Nakamura-Messenger for preparing the microtome sections. The manuscript benefited from careful reading and constructive contributions by Carolyn H. van der Bogert as well as from thorough reviews by Ulrich Ott, Frank J. Stadermann, and the associate editor Ian Lyon. This work was supported in part by the Deutsche Forschungsgemeinschaft through grant STE 576/17-1. The Stardust mission to comet 81P/Wild 2 was sponsored by NASA and executed jointly by the Jet Propulsion Laboratory and Lockheed Martin Space Systems. We are greatly indebted to many individuals who assured a successful comet encounter and who safely returned the Stardust collectors and their precious samples to Earth.

Editorial Handling—Dr. Ian Lyon

REFERENCES

Anders E. and Grevesse N. 1989. Abundances of the elements: Meteoritic and solar. *Geochimica et Cosmochimica Acta* 53:197–214.

Bradley J. P. 1994. Chemically anomalous, preaccretionally irradiated grains in interplanetary dust from comets. *Science* 265:925–929.

Brownlee D. E., Joswiak D. J., Love S. G., Bradley J. P., Nier A. O., and Schlutter D. J. 1994. Identification and analysis of cometary IDPs (abstract). 25th Lunar and Planetary Science Conference. pp. 185–186.

Brownlee D. E., Tsou P., Anderson J. D., Hanner M. S., Newburn R. L., Sekanina Z., Clark B. C., Hörz F., Zolensky M. E., Kissel J., McDonnell J. A. M., Sandford S. A., and Tuzzolino A. J. 2003. Stardust: Comet and interstellar dust sample return mission. *Journal of Geophysical Research* 108:E8111.

Brownlee D., Tsou P., Aléon J., Alexander C. M. O'D., Araki T., Bajt S., Baratta G. A., Bastien R., Bland P., Bleuet P., Borg J., Bradley J. P., Brearley A., Brenker F., Brennan S., Bridges J. C., Browning N. D., Brucato J. R., Bullock E., Burchell M. J., Busemann H., Butterworth A., Chaussidon M., Cheuvront A., Chi M., Cintala M. J., Clark B. C., Clemett S. J., Cody G., Colangeli L., Cooper G., Cordier P., Daghlian C., Dai Z., D'Hendecourt L., Djouadi Z., Dominguez G., Duxbury T., Dworkin J. P., Ebel D. S., Economou T. E., Fakra S., Fairey S. A. J., Fallon S., Ferrini G., Ferroir T., Fleckenstein H., Floss C., Flynn G., Franchi I. A., Fries M., Gainsforth Z., Gallien J.-P., Genge M., Gilles M. K., Gillet Ph., Gilmour J., Glavin D. P., Gounelle M., Grady M. M., Graham G. A., Grant P. G., Green S. F., Grossemy F., Grossman L., Grossman J. N., Guan Y., Hagiya K., Harvey R., Heck P., Herzog G. F., Hoppe P., Hörz F., Huth J., Hutcheon I. D., Ignatyev K., Ishii H., Ito M., Jacob D., Jacobsen C., Jacobsen S., Jones S., Joswiak D., Jurewicz A., Kearsley A. T., Keller L. P., Khodja H., Kilcoyne A. L. D., Kissel J., Krot A., Langenhorst F., Lanzirotti A., Le L., Leshin L. A., Leitner J., Lemelle L., Leroux H., Liu M.-C., Luening K., Lyon I., MacPherson G., Marcus M. A., Marhas K., Marty B., Matrajt G., McKeegan K., Meibom A., Mennella V., Messenger K., Messenger S., Mikouchi T., Mostefaoui S.,

Nakamura T., Nakano T., Newville M., Nittler L. R., Ohnishi I., Ohsumi K., Okudaira K., Papanastassiou D. A., Palma R., Palumbo M. E., Pepin R. O., Perkins D., Perronnet M., Pianetta P., Rao W., Rietmeijer F. J. M., Robert F., Rost D., Rotundi A., Ryan R., Sandford S. A., Schwandt C. S., See T. H., Schlutter D., Sheffield-Parker J., Simionovici A., Simon S., Sitnitsky I., Snead C. J., Spencer M. K., Stadermann F. J., Steele A., Stephan T., Stroud R., Susini J., Sutton S. R., Suzuki Y., Taheri M., Taylor S., Teslich N., Tomeoka K., Tomioka N., Toppani A., Trigo-Rodríguez J. M., Troadec D., Tsuchiyama A., Tuzzolino A. J., Tyliszczak T., Uesugi K., Velbel M., Vellenga J., Vicenzi E., Vincze L., Warren J., Weber I., Weisberg M., Westphal A. J., Wirick S., Wooden D., Wopenka B., Wozniakiewicz P., Wright I., Yabuta H., Yano H., Young E. D., Zare R. N., Zega T., Ziegler K., Zimmermann L., Zinner E., and Zolensky M. 2006. Comet 81P/Wild 2 under a microscope. *Science* 314:1711–1716.

Flynn G. J., Bleuet P., Borg J., Bradley J. P., Brenker F. E., Brennan S., Bridges J., Brownlee D. E., Bullock E. S., Burghammer M., Clark B. C., Dai Z. R., Daghlian C. P., Djouadi Z., Fakra S., Ferroir T., Floss C., Franchi I. A., Gainsforth Z., Gallien J.-P., Gillet Ph., Grant P. G., Graham G. A., Green S. F., Grossemy F., Heck P. R., Herzog G. F., Hoppe P., Hörz F., Huth J., Ignatyev K., Ishii H. A., Janssens K., Joswiak D., Kearsley A. T., Khodja H., Lanzirotti A., Leitner J., Lemelle L., Leroux H., Luening K., MacPherson G. J., Marhas K. K., Marcus M. A., Matrajt G., Nakamura T., Nakamura-Messenger K., Nakano T., Newville M., Papanastassiou D. A., Pianetta P., Rao W., Riekel C., Rietmeijer F. J. M., Rost D., Schwandt C. S., See T. H., Sheffield-Parker J., Simionovici A., Sitnitsky I., Snead C. J., Stadermann F. J., Stephan T., Stroud R. M., Susini J., Suzuki Y., Sutton S. R., Taylor S., Teslich N., Troadec D., Tsou P., Tsuchiyama A., Uesugi K., Vekemans B., Vicenzi E. P., Vincze L., Westphal A. J., Wozniakiewicz P., Zinner E., and Zolensky M. E. 2006. Elemental compositions of comet 81P/Wild 2 samples collected by Stardust. *Science* 314:1731–1735.

Hörz F., Bastien R., Borg J., Bradley J. P., Bridges J. C., Brownlee D. E., Burchell M. J., Chi M., Cintala M. J., Dai Z. R., Djouadi Z., Dominguez G., Economou T. E., Fairey S. A. J., Floss C., Franchi I. A., Graham G. A., Green S. F., Heck P., Hoppe P., Huth J., Ishii H., Kearsley A. T., Kissel J., Leitner J., Leroux H., Marhas K., Messenger K., Schwandt C. S., See T. H., Snead C., Stadermann F. J., Stephan T., Stroud R., Teslich N., Trigo-Rodríguez J. M., Tuzzolino A. J., Troadec D., Tsou P., Warren J., Westphal A., Wozniakiewicz P., Wright I., and Zinner E. 2006. Impact features on Stardust: Implications for comet 81P/Wild 2 dust. *Science* 314:1716–1719.

Leitner J., Stephan T., Kearsley A. T., Hörz F., Flynn G. J., and Sandford S. A. 2008. TOF-SIMS analysis of crater residues from Wild 2 cometary particles on Stardust aluminum foil. *Meteoritics & Planetary Science* 43. This issue.

Lodders K. and Fegley B., Jr. 1998. *The Planetary Scientist's Companion.* New York: Oxford University Press. 371 pp.

Sandford S. A., Aléon J., Alexander C. M. O'D., Araki T., Bajt S., Baratta G. A., Borg J., Bradley J. P., Brownlee D. E., Brucato J. R., Burchell M. J., Busemann H., Butterworth A., Clemett S. J., Cody G., Colangeli L., Cooper G., D'Hendecourt L., Djouadi Z., Dworkin J. P., Ferrini G., Fleckenstein H., Flynn G. J., Franchi I. A., Fries M., Gilles M. K., Glavin D. P., Gounelle M., Grossemy F., Jacobsen C., Keller L. P., Kilcoyne A. L. D., Leitner J., Matrajt G., Meibom A., Mennella V., Mostefaoui S., Nittler L. R., Palumbo M. E., Papanastassiou D. A., Robert F., Rotundi A., Snead C. J., Spencer M. K., Stadermann F. J., Steele A., Stephan T., Tsou P., Tyliszczak T., Westphal A. J., Wirick S., Wopenka B., Yabuta H., Zare R. N., and Zolensky M. E. 2006. Organics captured from comet 81P/Wild 2 by the Stardust spacecraft. *Science* 314:1720–1724.

Schramm L. S., Brownlee D. E., and Wheelock M. M. 1989. Major element composition of stratospheric micrometeorites. *Meteoritics* 24:99–112.

Stephan T. 2001. TOF-SIMS in cosmochemistry. *Planetary and Space Science* 49:859–906.

Stephan T., Klöck W., Jessberger E. K., Thomas K. L., Keller L. P., and Behla F. 1993. Multielement analysis of carbon-rich interplanetary dust particles with TOF-SIMS (abstract). *Meteoritics* 28:443–444.

Stephan T., Rost D., Vicenzi E. P., Bullock E. S., MacPherson G. J., Westphal A. J., Snead C. J., Flynn G. J., Sandford S. A., and Zolensky M. E. 2008. TOF-SIMS analysis of cometary matter in Stardust aerogel tracks. *Meteoritics & Planetary Science* 43. This issue.

Tsou P., Brownlee D. E., Sandford S. A., Hörz F., and Zolensky M. E. 2003. Wild 2 and interstellar sample collection and Earth return. *Journal of Geophysical Research* 108:E8113.

van der Bogert C. H., Golla-Schindler U., and Stephan T. 2007. HRTEM analyses of Stardust samples and their comparison with TOF-SIMS results (abstract). *Meteoritics & Planetary Science* 42:A153.

Zolensky M. E., Zega T. J., Yano H., Wirick S., Westphal A. J., Weisberg M. K., Weber I., Warren J. L., Velbel M. A., Tsuchiyama A., Tsou P., Toppani A., Tomioka N., Tomeoka K., Teslich N., Taheri M., Susini J., Stroud R., Stephan T., Stadermann F. J., Snead C. J., Simon S. B., Simionovici A., See T. H., Robert F., Rietmeijer F. J. M., Rao W., Perronnet M. C., Papanastassiou D. A., Okudaira K., Ohsumi K., Ohnishi I., Nakamura-Messenger K., Nakamura T., Mostefaoui S., Mikouchi T., Meibom A., Matrajt G., Marcus M. A., Leroux H., Lemelle L., Le L., Lanzirotti A., Langenhorst F., Krot A. N., Keller L. P., Kearsley A. T., Joswiak D., Jacob D., Ishii H., Harvey R., Hagiya K., Grossman L., Grossman J. N., Graham G. A., Gounelle M., Gillet Ph., Genge M. J., Flynn G., Ferroir T., Fallon S., Ebel D. S., Dai Z. R., Cordier P., Clark B., Chi M., Butterworth A. L., Brownlee D. E., Bridges J. C., Brennan S., Brearley A., Bradley J. P., Bleuet P., Bland P. A., and Bastien R. 2006. Mineralogy and petrology of comet 81P/Wild 2 nucleus samples. *Science* 314:1735–1739.